THE JOURNAL OF PHYSICAL CHEMISTRY A

ARTICLE

pubs.acs.org/JPCA

Ab Initio Reaction Rate Constants Computed Using Semiclassical Transition-State Theory: HO + H_2 → H_2O + H and Isotopologues

Thanh Lam Nguyen,[†,§] John F. Stanton,[‡,§] and John R. Barker*[,†]

[†]Department of Atmospheric, Oceanic and Space Sciences, University of Michigan, Ann Arbor, Michigan 48109-2143, United States

[‡]Department of Chemistry and Biochemistry, The University of Texas, Austin, Texas 78712-0165, United States

Supporting Information

ABSTRACT: A new algorithm [Nguyen, T. L.; Stanton, J. F.; Barker, J. R. Chem. Phys. Lett. 2010, 9, 499] for the semiclassical transition-state theory (SCTST) formulated by W. H. Miller and co-workers is used to compute rate constants for the isotopologues of the title reaction, with no empirical adjustments. The SCTST and relevant results from second-order vibrational perturbation theory (VPT2) are summarized. VPT2 is used at the CCSD(T) level of electronic structure theory to compute the anharmonicities of the fully coupled vibrational modes (including the reaction coordinate) of the transition structure. The anharmonicities are used in SCTST to compute the rate constants over the temperature range from 200 to 2500 K. The computed rate constants are compared to experimental data and theoretical calculations from the literature. The SCTST results for absolute rate constants and for both primary and secondary isotope effects are in excellent agreement with the experimental data for this reaction over the entire temperature range. The sensitivity of SCTST to various parameters is investigated by using a set of simplified models. The results show that multidimensional tunneling along the curved reaction path is important at low temperatures and the anharmonic coupling among the vibrational modes is important at high temperatures. The theoretical kinetics data are also presented as fitted empirical algebraic expressions.

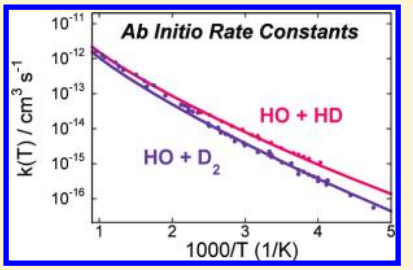

1. INTRODUCTION

The title reaction (and its reverse) is an important benchmark for kinetics and dynamics calculations.[1,2] In our previous paper (Paper I),[3] we described a practical implementation of semiclassical transition-state theory (SCTST), which was formulated by Miller and co-workers,[4−7] and applied it to the normal isotopic version of this reaction. In combination with second-order vibration perturbation theory (VPT2),[8] SCTST incorporates nonseparable coupling among all degrees of freedom and multidimensional quantum mechanical tunneling along the curved reaction path. By computing the cumulative reaction probability, both canonical and microcanonical reaction rate constants can be obtained.[3] The latter are particularly important for use in master equation calculations. The energy, geometry, and vibrational properties of the transition state were obtained from ab initio calculations carried out at very high levels of theory. To enable certain aspects of the calculations, the CFOUR quantum chemistry code was extended so that analytical gradients and vibrational anharmonicities could be computed for transition states at the CCSD(T) level of theory. The thermal rate constants computed in this way for the title reaction agreed within 10% with all of the available experimental data (i.e., over the temperature range from 200 to 2500 K).[3] We also compared the performance of SCTST with that of variational transition-state theory (VTST) as implemented in the POLYRATE computer program[9,10] and found that SCTST and VTST are of comparable accuracy, but the POLYRATE computer code required about twice as much computer time as the implementation of SCTST reported here.[3] In the present paper, we extend the SCTST calculations to other isotopologues of the HO + H_2 reaction and compare the results with experimental data and with other theoretical calculations from the literature (i.e., full-dimensional quantum dynamics, quasi-classical trajectory, and VTST). In addition, the VPT2 formulas for first-order saddle points that were used in CFOUR are summarized.

Not only is the HO + H_2 reaction an important benchmark for testing theories, but it is also the principal reaction controlling the concentration of atmospheric H_2[11] and is an important chain propagation step in H_2 combustion.[12] There is considerable interest in using hydrogen fuel to partly replace traditional fossil fuels.[13] It is expected that unburned H_2 released into the atmosphere will add to the atmospheric sources already present. These include oxidation of CH_4 and other volatile organic compounds, which produce formaldehyde as byproducts; photolysis of formaldehyde produces H_2.[14] The title reaction has been extensively studied both experimentally[15−20] and theoretically,[21−35] and its isotopic variants have been reviewed.[1,2] Generally, there is good agreement among the experiments and among the theoretical models, but some of the latter are more accurate than others.

Received: March 10, 2011
Revised: April 22, 2011
Published: May 03, 2011

Table 1. Calculated Vibrationally Adiabatic Barrier Heights (kcal mol^{-1}) for the HO + H_2 Reaction and Its Variant Isotopic Species Using the HEAT Protocol

reaction	ΔV_a (ZPE_h)	ΔV_a (ZPE_{anh})	$\Delta\Delta V_a$[a]
HO + H_2 = H_2O + H	5.83	5.88	0.05
HO + HD = H_2O + D	5.67	5.70	0.03
HO + DH = HOD + H	6.06	6.05	0.01
HO + D_2 = HOD + D	6.01	5.98	−0.03
DO + H_2 = DOH + H	5.54	5.62	0.08
DO + HD = DOH + D	5.37	5.44	0.07
DO + DH = D_2O + H	5.76	5.78	0.02
DO + D_2 = D_2O + D	5.70	5.71	0.01

[a] Difference in computed barrier heights: $\Delta\Delta V_a = \Delta V_a(ZPE_{anh}) - \Delta V_a(ZPE_h)$

This paper is organized as follows. In section 2, the SCTST method is briefly sketched, and the ab initio calculations and VPT2 transition-state formulas are summarized. Computed thermal rate constants and kinetic isotope effects (KIEs) are presented in section 3. Finally, conclusions are given in section 4.

2. METHODOLOGY

2.1. Ab Initio Calculations. Geometries and harmonic vibrational frequencies of all stationary points in the $H_2 + OH \rightarrow H + H_2O$ reaction and its isotopic variants were obtained using coupled-cluster theory involving single, double, and a perturbative treatment of triple excitations (CCSD(T)),[36] in combination with atomic natural orbital basis sets,[37] truncated to 4s3p2s1f for oxygen and 4s2p1d for hydrogen; this basis is hereafter designated as ANO1. Anharmonic force fields were computed at the CCSD(T)/ANO1 level of theory for all species (H_2, OH, H_2O, the transition structures, and their isotopic variants) using VPT2. In all cases where harmonic frequencies are within 100 cm^{-1} of zeroth-order level positions corresponding to two quantum transitions (potential Fermi resonances), standard deperturbation techniques were applied. In all of these calculations, the core electrons were kept frozen.

Energies of all species considered were refined using high-accuracy extrapolated ab initio thermochemistry (HEAT-345Q, hereinafter denoted as HEAT) theory.[38−40] HEAT contains a very high level treatment of electron correlation effects, extending beyond the coupled-cluster singles, doubles, and triples model. In the calculations presented here, the highest applied level of electron correlation is CCSDTQ. In addition, other small corrections are made, including the anharmonic zero-point vibrational energy (ZPE), a scalar relativistic correction, first-order spin−orbit effects, and the diagonal Born−Oppenheimer correction. The HEAT total energy is subsequently computed as

$$E_{HEAT} = E_{HF}^{\infty} + \Delta E_{CCSD(T))}^{\infty} + \Delta E_{CCSDT} + \Delta E_{HLC} + \Delta E_{REL} + \Delta E_{ZPE} + \Delta E_{DBOC} + \Delta E_{SO} \quad (1)$$

where the terms are defined in the original papers.[38−40] In the present work, the experimental spin−orbit stabilization of −38.2 cm^{-1} for HO radical is adopted (see discussion in ref 40); the first-order spin−orbit corrections for all other relevant species vanish.

From the HEAT protocol, the reaction enthalpy at 0 K for the $H_2 + OH \rightarrow H + H_2O$ reaction is computed to be −14.35 kcal mol^{-1}, within the uncertainty of the experimental value of −14.33 ± 0.04 kcal mol^{-1} (see ref 3). It is expected that an accuracy within ∼0.2 kcal mol^{-1} is achieved for the computed reaction barrier heights, which are tabulated in Table 1. The results in Table 1 show that the computed barrier heights change slightly (<0.1 kcal mol^{-1}) when anharmonic ZPEs are included instead of harmonic ZPEs. These small changes nevertheless affect the computed thermal rate constants significantly at low temperatures but negligibly at high temperatures. For example, a shift of a barrier height by 0.1 kcal mol^{-1} alters the computed thermal rate by ∼30% at 200 K but only by ∼2% at 2500 K.

In this work, Gaussian[41] and CFOUR[42] quantum chemistry programs were used for all calculations.

2.2. Semiclassical Transition-State Theory. As described in Paper I, the SCTST of Miller and co-workers[4−7] expresses the microcanonical and canonical rate constants as follows

$$k(E) = \frac{1}{h}\frac{G^{\ddagger}(E)}{\rho(E)} \quad (2)$$

$$k(T) = \frac{1}{h}\frac{\int_{-\infty}^{\infty} G^{\ddagger}(E)\exp(-E/k_BT)\,dE}{Q_{re}(T)} \quad (3a)$$

where h is Planck's constant, k_B is Boltzmann's constant, T is the temperature, $\rho(E)$ is the density of states of the reactant, Q_{re} is the total partition function of the reactant(s), and $G^{\ddagger}(E)$ is the cumulative reaction probability (CRP).[4] The center of mass translations are rigorously separable. At temperatures that are not too high, it is a good approximation to treat the rotations around the principal axes as separable, so that eq 3a can be written

$$k(T) = \frac{1}{h}\frac{Q_t^{\ddagger}Q_r^{\ddagger}}{Q_tQ_r}\frac{\int_{-\infty}^{\infty} G_v^{\ddagger}(E_v)\exp(-E_v/k_BT)\,dE_v}{Q_v(T)} \quad (3b)$$

in which vibrational energy E_v is the variable of integration. The corresponding CRP is given by

$$G_v^{\ddagger}(E_v) = \sum_{n_1}\sum_{n_2}\cdots\sum_{n_{F-2}}\sum_{n_{F-1}} P_n(E_v) \quad (4)$$

The semiclassical tunneling probability P_n is given by[6]

$$P_n(E) = \frac{1}{1+\exp[2\theta(\mathbf{n},E)]} \quad (5)$$

where the barrier penetration integral $\theta(\mathbf{n},E)$ and related quantities are given by

$$\theta(\mathbf{n},E) = \frac{\pi\Delta E}{\Omega_F}\frac{2}{1+\sqrt{1+4x_{FF}\Delta E/\Omega_F{}^2}} \quad (6)$$

$$\Delta E = \Delta V_o + G_o - E + \sum_{k=1}^{F-1}\omega_k\left(n_k+\frac{1}{2}\right) + \sum_{k=1}^{F-1}\sum_{l=k}^{F-1}x_{kl}\left(n_k+\frac{1}{2}\right)\left(n_l+\frac{1}{2}\right) \quad (7)$$

$$\Omega_F = \overline{\omega}_F - \sum_{k=1}^{F-1}\overline{x}_{kF}\left(n_k+\frac{1}{2}\right) \quad \text{with} \quad \overline{\omega}_F = -i\omega_F \quad \text{and} \quad \overline{x}_{kF} = ix_{kF} \quad (8)$$

In these expressions, F is the number of internal degrees of freedom of the transition state, ordered so that the reaction

dx.doi.org/10.1021/jp2022743 |J. Phys. Chem. A 2011, 115, 5118–5126

coordinate is last (i.e., has index F); ω_k is the harmonic vibrational frequency, ω_F is the imaginary frequency associated with the reaction coordinate, x_{kl} are the anharmonicity constants that involve coupling among the orthogonal degrees of freedom, x_{kF} are the (pure imaginary) coupling terms between the reaction coordinate and the orthogonal degrees of freedom, x_{FF} is the (real-valued) anharmonicity constant for the reaction path, and ΔV_o is the classical barrier height. The term G_o is a constant, which is irrelevant in spectroscopic measurements (where only energy differences are important) but that must be included for thermochemistry.[43] In this paper and in Paper I, terms labeled as ZPEs always include the term G_0.

The reaction barrier height is often expressed as the difference between the ZPE of the transition state and that of the reactant-(s) (i.e., the vibrationally adiabatic ground-state potential energy difference $\Delta V_a^{G\ddagger}$)

$$\Delta V_a^{G\ddagger} = \Delta V_0 + E_z - E_z^R \tag{9}$$

where the ZPEs for the $F-1$ degrees of freedom orthogonal to the reaction coordinate in the transition state and the F degrees of freedom in the reactant(s) are given by E_z and E_z^R, respectively

$$E_z = G_0 + \frac{1}{2}\sum_{k=1}^{F-1}\omega_k + \frac{1}{4}\sum_{k=1}^{F-1}\sum_{l=k}^{F-1}x_{kl} \tag{10a}$$

$$E_z^R = G_0^R + \frac{1}{2}\sum_{k=1}^{F}\omega_k^R + \frac{1}{4}\sum_{k=1}^{F}\sum_{l=k}^{F}x_{kl}^R \tag{10b}$$

The superscript R denotes parameters corresponding to the reactant(s), and quantities without the superscript correspond to the transition state.

In many cases, it is convenient to choose the zero of energy as the ZPE of the reactant(s) instead of at the electronic energy of the reactant(s). The energy relative to the ZPE of the reactant(s) is $E' = E - E_z^R$, where E is the electronic energy of the reactant(s). By substituting this expression for E in eq 7 and making use of eqs 9 and 10a, the following alternative expression for eq 7 is obtained

$$\Delta E = \Delta V_a^{G\ddagger} + G_0 - (E' + E_z) + \sum_{k=1}^{F-1}\omega_k\left(n_k+\frac{1}{2}\right) + \sum_{k=1}^{F-1}\sum_{l=k}^{F-1}x_{kl}\left(n_k+\frac{1}{2}\right)\left(n_l+\frac{1}{2}\right) \tag{11}$$

Equations 7 and 11 are equivalent, and one or the other may be more convenient for a given application. We find eq 11 to be convenient for kinetics calculations in which partition functions or densities of states are computed at energies relative to the ZPE of the reactant(s).

The algorithm described in Paper I and used to compute the CRP is based on the algorithms of Wang and Landau[44] and of Basire et al.,[45] as extended by Nguyen and Barker.[46] The basic idea is to obtain average values of the parameters $\langle\Delta E\rangle$ and $\langle\Omega_F\rangle$ for each energy bin by sampling the states in each bin. The accuracy of the averages can be improved by increasing the number of samples. The average parameters are then used in eq 5 to compute an average value for the tunneling probability $\langle P(E_i)\rangle$ for the energy bin with energy E_i. The CRP is the cumulative sum of the probabilities and can be used in eq 2 to compute $k(E)$ for master equation simulations. It can also be used in eq 3 to compute thermal rate constants. A computer program (program "sctst") incorporating the algorithm has been made public as part of the MultiWell Program Suite.[47,48]

2.3. Second-Order Vibrational Perturbation Theory for Transition Structures. The procedure for incorporating the anharmonicity constants at the transition state into SCTST was detailed by Hernandez et al.[7] and will be briefly summarized here. One begins with the usual VPT2 expression for the energy of a vibrational state with quantum numbers $(n_1, n_2, ...)$, namely

$$E = G_0 + \sum_k \omega_k\left(n_k+\frac{1}{2}\right) + \sum_{k=1}\sum_{l=k}x_{kl}\left(n_k+\frac{1}{2}\right)\left(n_l+\frac{1}{2}\right) \tag{12}$$

Applied to a transition state (where the VPT2 vibrational energy is complex-valued), the energy of a state with quantum numbers (n) relative to the potential energy of the reactants can be written in the partitioned form

$$E = \Delta V_0 + G_0 + \sum_{k=1}^{F-1}\omega_k\left(n_k+\frac{1}{2}\right) + \sum_{k=1}^{F-1}\sum_{l=k}^{F-1}x_{kl}\left(n_k+\frac{1}{2}\right)\left(n_l+\frac{1}{2}\right) + \omega_F\left(n_F+\frac{1}{2}\right) + \sum_{k=1}^{F-1}x_{kF}\left(n_k+\frac{1}{2}\right)\left(n_F+\frac{1}{2}\right) + x_{FF}\left(n_F+\frac{1}{2}\right)^2 \tag{13}$$

where the summations exclude the reaction coordinate (index number F). Then, one invokes the semiclassical approximation for the barrier penetration integral $\theta(\mathbf{n},E)$

$$\frac{i\theta(\mathbf{n},E)}{\pi} = \left(n_F+\frac{1}{2}\right) \tag{14}$$

and inserts this into eq 13, yielding

$$E = \Delta V_0 + G_0 + \sum_{k=1}^{F-1}\omega_k\left(n_k+\frac{1}{2}\right) + \sum_{k=1}^{F-1}\sum_{l=k}^{F-1}x_{kl}\left(n_k+\frac{1}{2}\right)\left(n_l+\frac{1}{2}\right) + \frac{i\theta(\mathbf{n},E)}{\pi}\left[\omega_F + \sum_{k=1}^{F-1}x_{kF}\left(n_k+\frac{1}{2}\right)\right] - \frac{x_{FF}}{\pi^2}\theta(\mathbf{n},E)^2 \tag{15}$$

Using the definitions from the previous section, this expression is equivalent to the following quadratic equation for the barrier penetration integral $\theta(\mathbf{n},E)$

$$0 = \Delta E - \frac{\Omega_F}{\pi}\theta(\mathbf{n},E) - \frac{x_{FF}}{\pi^2}\theta(\mathbf{n},E)^2 \tag{16}$$

for which eq 6 of the previous section is the meaningful solution.

The anharmonicity constants that are central to VPT2 were given by Hernandez et al. in the normal coordinate representation,[7] with separate cases for those carrying the reaction coordinate as an index. Although equivalent to those expressions, the equations given below are simpler in form and apply to cases including local minima, transition states, and higher-order saddle points (if indeed any use for the latter exists). Using the shorthand notations

$$\overline{\omega}_k = ||\omega_k|| \tag{17a}$$

$$\overline{\delta}_k = (-1)^{\delta_{Fk}} \tag{17b}$$

$$\overline{\overline{\delta}}_k = -i\delta_{kF} + (1 - \delta_{kF}) \tag{17c}$$

and the modified form of dimensionless normal coordinate force constants

$$\overline{\phi}_{ijk\ldots} \equiv C\frac{f_{ijk\ldots}}{(\overline{\omega}_i\overline{\omega}_j\overline{\omega}_k\ldots)^{1/2}} \tag{18}$$

(the *fijk*... are the force constants used in the expressions of Hernandez et al.[7]), it is easy to show that the expressions

$$x_{kk} = \frac{\overline{\phi}_{kkkk}\overline{\delta}_k}{16} - \sum_m \frac{8\overline{\omega}_k^2\overline{\delta}_k - 3\overline{\omega}_m^2\overline{\delta}_m}{16\overline{\omega}_m(4\overline{\omega}_k^2\overline{\delta}_k - \overline{\omega}_m^2\overline{\delta}_m)}\overline{\phi}_{kkm}^2\overline{\delta}_m\overline{\delta}_k \tag{19}$$

and

$$x_{kl} = \overline{\overline{\delta}}_{kt}\overline{\overline{\delta}}_{lt}\left[\frac{\overline{\phi}_{kkll}}{4} - \sum_m\left(\frac{\overline{\phi}_{kkm}\overline{\phi}_{llm}\overline{\delta}_m}{4\overline{\omega}_m} - \frac{\overline{\phi}_{klm}^2\overline{\omega}_m}{2\Omega_{klm}}\right) + \left(\overline{\delta}_k\frac{\overline{\omega}_k}{\overline{\omega}_l} + \overline{\delta}_l\frac{\overline{\omega}_l}{\overline{\omega}_k}\right)\sum_\alpha^{xyz} B_\alpha(\zeta_{kl}^\alpha)^2\right] \tag{20}$$

where

$$\Omega_{klm} = \frac{(\overline{\omega}_k^2\overline{\delta}_k + \overline{\omega}_l^2\overline{\delta}_l - \overline{\omega}_m^2\overline{\delta}_m)^2 - 4\overline{\omega}_k^2\overline{\omega}_l^2\overline{\delta}_k\overline{\delta}_l}{(\overline{\omega}_k^2\overline{\delta}_k + \overline{\omega}_l^2\overline{\delta}_l - \overline{\omega}_m^2\overline{\delta}_m)} \tag{21}$$

reduce to the usual VPT2 expressions for the ground state as well as to those of ref 6 for transition states. Together with the expression for the G_0 constant term

$$G_0 = \sum_k\left(\frac{\overline{\phi}_{kkkk}\overline{\delta}_k}{64} - \frac{7\overline{\phi}_{kkk}^2}{576\overline{\omega}_k}\right) + \frac{3}{64}\sum_{k\neq l}\frac{\overline{\omega}_l\overline{\phi}_{kkl}^2\overline{\delta}_k}{4\overline{\omega}_k^2\overline{\delta}_k - \overline{\omega}_l^2\overline{\delta}_l} - \frac{1}{4}\sum_{k<l<m}\frac{\overline{\phi}_{klm}^2\overline{\omega}_k\overline{\omega}_l\overline{\omega}_m}{(\overline{\omega}_k^2\overline{\delta}_k + \overline{\omega}_l^2\overline{\delta}_l - \overline{\omega}_m^2\overline{\delta}_m) - 4\omega_k{}^2\omega_l{}^2\overline{\delta}_k\overline{\delta}_l} - \frac{1}{4}\sum_\alpha(B_e^\alpha + \sum_{kl}B_e^\alpha\zeta_{kl}^\alpha\zeta_{kl}^\alpha) \tag{22}$$

this is a full documentation of the equations used by VPT2 for transition states in this work. Finally, we note that the usual deperturbation technique of excluding terms with "small" denominators (potential Fermi resonances; see section 2.1 of this paper) must be extended to both the anharmonicity constants and the G_0 term. The ZPE of the orthogonal modes in the transition state (eq 10 from previous section) is invariant to such deperturbation, although the individual values of G_0 and the anharmonicity constants are shifted by this process. This invariance provides a valuable test for checking the computational implementation of these equations.

3. RESULTS AND DISCUSSION

3.1. Simplified models for OH + H_2. The results for the normal isotopologue of the reaction were reported previously. In the present paper, we investigate the sensitivity of the computed CRP (and thermal reaction rate constants) to some of the vibrational anharmonicity constants. For this reason, we investigated various approximate models produced by omitting some of the terms in eqs 7 and 8.

Table 2. Approximate Models Defined According to the Terms Included in Equations 7 and 8

type	ω_e	ω_F	x_{kk}	x_{kl}	x_{kF}	x_{FF}	other	ΔV_a (kcal mol^{-1})
Model-1	x							5.56
Model-2	x	x						5.56
Model-3	x	x					x[a]	5.56
Model-4	x	x				x		5.56
Model-5	x	x			x	x		5.56
Model-6	x	x	x			x		5.81
Model-7	x	x	x		x	x		5.81
Model-8	x	x	x	x	x	x		5.88

[a] Includes tunneling corrections for an unsymmetrical Eckart barrier.

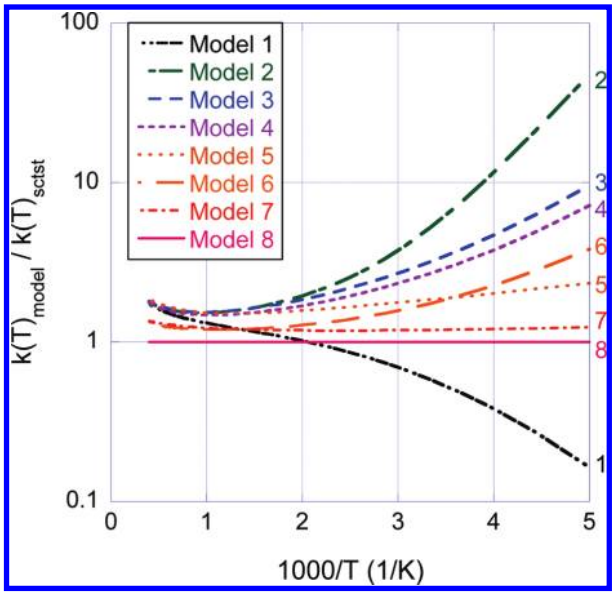

Figure 1. Thermal rate constants as a function of temperature calculated using various approximate models for the OH + H_2 reaction, relative to the thermal rate constant computed using the SCTST.

Eight models were defined, ranging from the simplest (Model 1), which corresponds to conventional harmonic canonical TST without tunneling corrections but including ZPE corrections. The most elaborate model is the full SCTST approach (Model 8). The models are defined in Table 2.

To assess the quality of the models, the thermal vibrational partition functions (which are proportional to the thermal rate constants) computed with each model were divided by that from the SCTST approach (Model 8); the ratios of corresponding thermal rate constants are shown versus temperature in Figure 1.

Because the ZPEs calculated using eq 10 vary from one model to another depending on which anharmonic terms are included, the vibrationally adiabatic barrier heights also vary (see Table 2). The barrier heights fall into three groups. The full SCTST (Model 8), which includes all anharmonicities for the orthogonal vibrations, predicts the highest vibrationally adiabatic barrier. When off-diagonal anharmonicities are neglected (Models 6 and 7), the barrier is a little lower. When both diagonal and off-diagonal anharmonicity terms are neglected (Models 1−5), the

dx.doi.org/10.1021/jp2022743 |J. Phys. Chem. A 2011, 115, 5118–5126

barrier is lowest. The effects of barrier height are most apparent at temperatures at around 1000 K in Figure 1, where the model results are seen to fall into three distinct groups.

The other differences apparent in Figure 1 are mostly due to differences in tunneling corrections, as discussed in the following paragraphs. Note that Model 8 is the full SCTST.

Model 1 (TST). Because tunneling is neglected, this method grossly underestimates the rate constant at low temperatures. Conversely, it overestimates the rate constant at higher temperatures, mostly due to its neglect of vibrational anharmonicity.

Model 2. This model corresponds to conventional harmonic TST but includes quantum tunneling through an inverted parabolic barrier, as was first described by Wigner.[49] Although the trends are qualitatively correct, the rate constants predicted using this model are too large because tunneling is greatly overestimated.

Model 3 (TST/Eckart). This model corresponds to conventional harmonic TST but includes quantum tunneling through an unsymmetrical Eckart potential barrier,[50−52] which was parametrized in terms of the energy barriers (forward and reverse directions) and the imaginary frequency. This model does not correspond to any simplified SCTST approach but is included for comparison because it is a popular method. At low temperatures, the effect of tunneling is again greatly overestimated.

Model 4. This model is derived from the SCTST approach by including only the harmonic vibrational frequencies (including the imaginary frequency) and the diagonal anharmonicity coefficient for the reaction coordinate (i.e., the x_{FF} term). This model gives results that are slightly better than those of Model 3.

Model 5. This model is the same as Model 4, except that it also includes the anharmonic coupling between the reaction coordinate and the other vibrations (i.e., the x_{kF} terms). By including this coupling, the model takes into account multidimensional reaction path curvature,[6] which has been discussed extensively.[9,52−57] This model performs considerably better than Models 3 and 4 at low temperatures, indicating that multidimensional reaction path curvature is important for this reaction.

Model 6. This is the same as Model 4, except that it also includes the diagonal anharmonicity terms for the orthogonal vibrations. Because all off-diagonal anharmonicities are neglected, it is a separable approximation to the SCTST. This model performs better than Model 4; by including the anharmonicities, the barrier height is more nearly equal to the barrier height of Model 8.

Model 7. This model is the same as the complete SCTST, except that the off-diagonal anharmonicity terms (i.e., the x_{kl} terms) for the orthogonal vibrations are neglected. Model 7 agrees (to within 25%) with Model 8 over the entire temperature range. The corresponding lines in Figure 1 are nearly parallel at low temperatures, indicating that coupling among the orthogonal vibrations has essentially no effect on the tunneling corrections.

In summary, the ZPE differences associated with each model produce different barrier heights and small deviations in the rate constant. At low temperatures, tunneling is dominant and must be treated as rigorously as possible. Thus, to achieve the best results for this reaction, all anharmonicities associated with the reaction coordinate must be included.

3.2. HO + HD → Products. This reaction proceeds via two channels

$$HO + HD \rightarrow HOH + D \quad (23a)$$

$$HO + DH \rightarrow HOD + H \quad (23b)$$

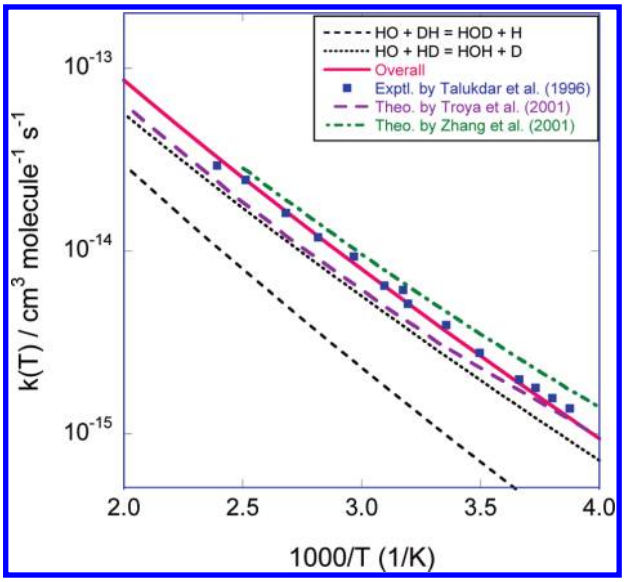

Figure 2. Thermal rate constants of the HO + HD/DH reactions as a function of temperature.

Talukdar et al. used CW Lyman-α resonance fluorescence to investigate the reactions above and obtained H-atom yields of 0.17 ± 0.03 and 0.26 ± 0.05 at 250 and 298 K, respectively, for each OH radical consumed.[18] The full-dimensional quantum dynamic calculations performed by Zhang et al. and based on the YZCL2 potential energy surface (PES) produced values of 0.17 and 0.23, respectively, in excellent agreement with the measurements.[30] Recently, using the same PES, Garcia et al.[32] carried out quasi-classical trajectory calculations (QCTs) and obtained 0.29 for the relative yield of H-atoms at 298 K, also in excellent agreement with experiment. In the present work, the SCTST approach obtains relative yields of 0.24 and 0.27 at 250 and 298 K, respectively, in excellent agreement with all of the experimental and theoretical results.

Overall thermal rate constants for reaction 23 were measured by Talukdar et al. between 248 and 418 K using pulsed photolysis to generate OH and laser-induced fluorescence to monitor the subsequent OH decay.[18] The results (see Figure 2) show very little scatter. This reaction has been investigated using various theoretical techniques and various PESs. While Troya et al.[33] used VTST and the WSLFH PES surface,[28] Zhang et al.[30] used a full-dimensional quantum dynamic treatment on the YZCL2 PES,[29] which was constructed by using the CCSD(T)/aug-cc-pVQZ level of theory. Note that the classical barrier height derived from the YZCL2 PES is 5.40 kcal mol^{-1},[29] nearly identical to the HEAT value obtained in the present work, 5.39 kcal mol^{-1} (specifically, 5.28 plus 0.11 kcal mol^{-1} from the experimental spin−orbit correction for the HO radical). Thermal rate constants for reaction 23 were also obtained in the present work as a function of temperature. All of these results are plotted in Figure 2.

Inspection of Figure 2 shows that the predictions of Troya et al.[33] using the ICVT/μOMT approach underestimate the experimental result by ∼30% from 250 to 420 K, and the calculations of Zhang et al.[30] overestimate the measurements by ∼20%. In contrast, the SCTST results obtained in the present work agree with the experimental data[18] within the experimental uncertainties (∼7%) over the entire temperature range. The SCTST results reported in Paper I are also in good agreement

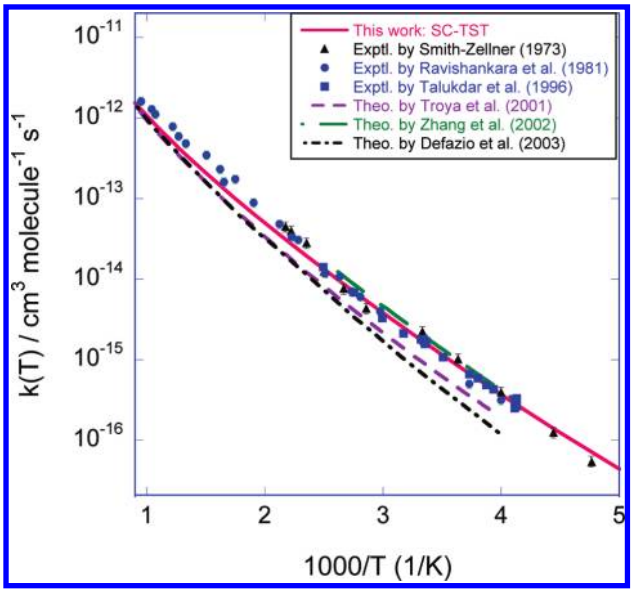

Figure 3. Thermal rate constants of the HO + D_2 reaction as a function of temperature.

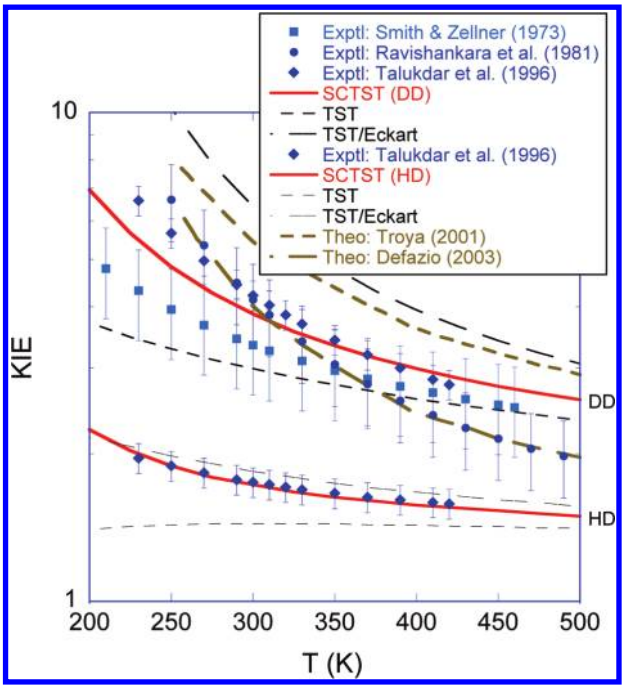

Figure 4. Kinetic isotopic effect (KIE) for the HO + D_2 and HO + HD reactions (labeled on the right-hand margin) as a function of temperature.

with the experimental data reported by several groups, although the data are not entirely consistent. The KIE is defined as the ratio of the thermal rate constant for the lighter isotopologue to that for the heavier one, that is, KIE = $k(HO+H_2)/k(HO+HD)$. The KIEs predicted by SCTST tend to split the difference between the experimental data sets obtained by different groups (see Figure 4).

3.3. HO + D_2 → HOD + D. This reaction has been studied both experimentally and theoretically. Three sets of experimental thermal rate constants cover the range of temperatures from 210 up to 1050 K.[17,18,58] In the temperature range from 250 to 400 K, which is most relevant to atmospheric chemistry and where the three studies overlap, the measurements agree within 10%. Three theoretical studies were carried out prior to the present work. Troya et al.[33] and Zhang[31] employed the techniques mentioned in section 3.2, while Defazio et al.[34] carried out a quantum dynamics study on the WSLFH potential energy surface. All of these data and the SCTST results are presented in Figure 3 for comparison.

Inspection of Figure 3 shows that the calculated rate constants of Troya et al.[33] and Defazio et al.[34] are lower than the experimental results, whereas those of Zhang[31] are slightly higher. Although the rate constants calculated using SCTST are a little lower than the measurements at temperatures above 400 K, they agree within 10% with all of the experimental data. Figure 3 also shows that the SCTST approach reproduces the rate constants reported by Talukdar et al.[18] within the quoted experimental uncertainty of ~5%.

The theoretical KIEs computed in this work are shown in Figure 4 along with those derived from the measured rate constants. The theoretical KIE curves reported earlier by Troya et al.[33] and Defazio et al.[34] are also included for comparison. Note that because the rate constants for HO + H_2 and HO + D_2 were not measured at exactly the same temperatures, the analytical expressions provided in the original papers as fits to the data were used to compute the KIEs. The experimental errors in the KIEs were estimated by propagation of errors, based on the standard deviations reported in the original papers for the measured rate constants.

Measurement of KIEs is challenging because they depend on the ratio of two measurements and minor discrepancies may become exaggerated. It is clear from Figure 4 that the experiments of Smith and Zellner[58] are in only moderate agreement with those of Talukdar et al.[18] and Ravishankara et al.,[17] but the latter two data sets are in good agreement with each other. The KIEs calculated in the present work tend to fall between the experimental data of Smith and Zellner and the combined data of Ravishankara et al. and Talukdar et al. at temperatures below 350 K. At temperatures above 400 K, the present results are higher than those of the experiments, but the deviations are small (within 2 standard deviations). The KIEs calculated by Troya et al.,[33] who used the ICVT/μOMT approach, are significantly larger than all of the experimental data, while those determined by Defazio et al.[34] using the quantum dynamics calculations are in excellent agreement with the experimental results of Ravishankara et al. and in very good agreement with those of Talukdar et al. It is worth noting that although both Troya et al. and Defazio et al. used the same potential energy surface, the KIEs calculated using the two different methods are not in good agreement with each other.

Also shown in Figure 4 are calculations carried out using Model 1 (TST) and Model 3 (TST/Eckart). Both TST and TST/Eckart are widely used because they are simple, convenient, and fairly reliable. However, quantum effects are very important in the HO + H_2 reaction system, posing a serious challenge to simple models. Nonetheless, it is interesting to examine the simple models because it is at least plausible that systematic errors tend to cancel when computing KIEs. To check this possibility, we computed KIEs as a function of temperature for both of the HO + HD and HO + D_2 reactions using three different approaches involving TST, TST/Eckart, and SCTST. Inspection of Figure 4 shows that TST underestimates the experimental values for both reactions, whereas TST/Eckart

dx.doi.org/10.1021/jp2022743 |J. Phys. Chem. A 2011, 115, 5118–5126

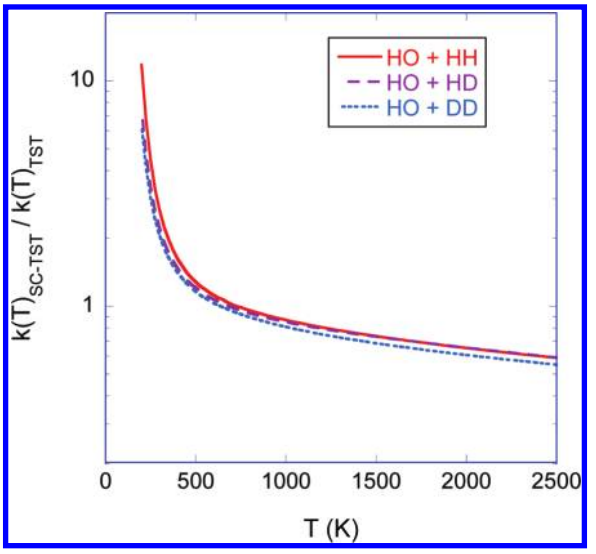

Figure 5. Ratios of SCTST and TST thermal rate constants as a function of temperature.

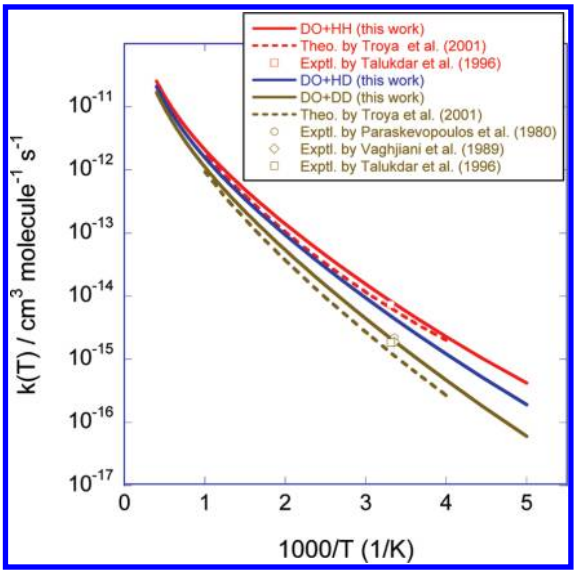

Figure 6. Thermal rate constants for the reactions of DO with H_2, HD, and D_2 as a function of temperature.

overestimates them significantly for HO + D_2, especially at low temperatures where tunneling is most important. For HO + HD, TST/Eckart agrees within the error bars. For both reactions, SCTST is much more accurate than the simple models.

To further examine the effects of tunneling, ratios of the rate constant calculated using SCTST and TST for the reactions of HO with H_2, HD, and D_2 are plotted as functions of temperature in Figure 5. SCTST performs well at low temperatures because it includes multidimensional quantum mechanical tunneling. It performs well at high temperatures because it includes nonseparable anharmonicites, which produce more accurate descriptions of relatively high energy vibrational states. Figure 5 shows that the calculated ratios decrease sharply as the temperature increases from 200 to 500 K and more slowly at higher temperatures. At low temperatures, the reactions proceed mostly by tunneling through the potential energy barriers. For example, at T = 200 K, about 92, 88, and 86% of the total of chemically reactive fluxes for the corresponding reactions of HO with H_2, HD, and D_2 arises from tunneling. As the temperature is increased, tunneling becomes less important while anharmonicity becomes more important. At 2500 K, for example, tunneling is insignificant, while anharmonicity reduces the rate constants by ~40%.

3.4. DO + H_2/HD/D_2 Reactions. The H-atom in the hydroxyl radical reactant does not participate directly in the reaction. Nonetheless, the presence of the H-atom affects the vibrational energy levels, rotational constants, and mass of the reactant; it therefore has some influence on the computed rate constants. When the H-atom is replaced by a D-atom, the reaction rate constant is affected. This secondary isotope effect was investigated by computing thermal rate constants and KIEs for the reactions of DO with H_2, HD, and D_2 (relative to the corresponding reactions of HO). The computed rate constants and data from the literature[18,59,60] are plotted in Figure 6. The experimental data are only available near room temperature. The rate constants computed using SCTST agree well with the experimental data.

The KIEs for the reactions are shown in Figure 7, which shows that they increase rapidly with temperature up to about 700 K, where they become almost constant at values a little lower than unity. In other words, the reactions of DO are slightly faster than

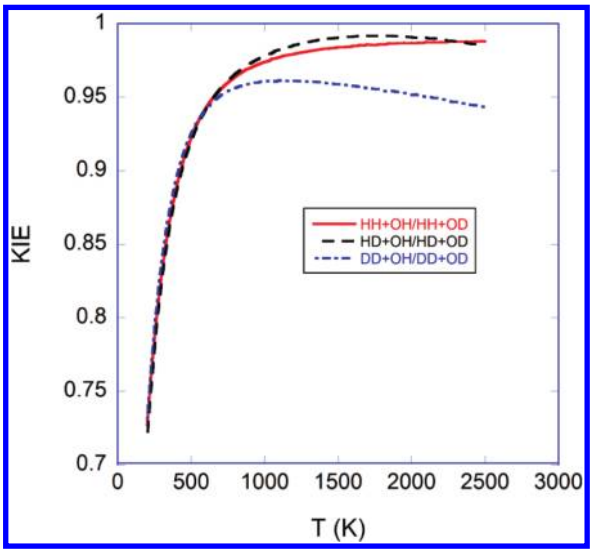

Figure 7. Ratios of thermal rate constants as a function of temperature between the reactions of HO and the corresponding reactions of DO with H_2, HD, and D_2.

those of HO, especially at low temperatures. As mentioned above, these differences originate from small differences in ZPEs (0.26 kcal mol^{-1}), rovibrational parameters, and anharmonicity constants.

At temperatures below ~500 K, where tunneling is dominant, the three curves in Figure 7 are almost indistinguishable. This suggests that the reactions are affected quite similarly by substitution of DO for HO. We surmise that tunneling is not influenced significantly by the "spectator" atom attached to the oxygen in the hydroxyl radical, but the temperature variation of the curves arises from minor shifts in the ZPE and changes in rotational constants. At high temperature, where the KIEs become almost independent of temperature, the ZPE differences are negligible relative to k_BT, but differences in rotational constants may account for the difference from unity.

dx.doi.org/10.1021/jp2022743 |J. Phys. Chem. A 2011, 115, 5118–5126

Table 3. Thermal Rate Constants for Isotopologues of the HO + H_2 Reaction Fitted (from 200 to 2500 K) to the Expression $k(T) = A \times T^c \times \exp(-B/T)$ cm^3 molecule^{-1} s^{-1}

reaction	A	c	B
HO + H_2	4.2×10^{-17}	1.78	1453
HO + HD	3.2×10^{-17}	1.80	1627
HO + D_2	3.3×10^{-17}	1.77	1830
DO + H_2	2.8×10^{-17}	1.83	1419
DO + HD	2.0×10^{-17}	1.86	1525
DO + D_2	1.6×10^{-17}	1.87	1724

For convenience, the thermal rate constants for the reactions computed using the SCTST were fitted to eq 12 in the temperature range from 200 to 2500 K, and the fitted parameters (A, c, and B) are summarized in Table 3.

$$k(T) = AT^c \exp(-B/T) \quad (24)$$

4. SUMMARY AND CONCLUSIONS

In this work, thermal rate constants and kinetic isotopic effects for the HO + H_2 reaction and its isotopologues were computed using SCTST. The necessary input data, including rovibrational parameters, anharmonic constants, and reaction barriers, were obtained at accurate levels of theory. In particular, energy parameters were obtained using the HEAT protocol, and the vibrational parameters were obtained using CCSD(T)/ANO1 and VPT2 theory as implemented for this purpose in the CFOUR program. The computed SCTST values are in excellent agreement with the experimental data, which span a wide range of temperatures. Moreover, the SCTST results for this reaction are slightly superior to the best theoretical results in the literature.

It is likely that the excellent performance of the present SCTST calculations is mainly due to two facts: (a) the SCTST accounts for full nonseparability of the coordinates and multidimensional tunneling, and (b) a high level of electronic structure theory was used to calculate the reaction barrier heights and vibrational anharmonicities.

Although the SCTST has produced accurate ab initio rate constants for this reaction, it is important to consider its possible limitations. Because SCTST is based on TST, which assumes that there is no "recrossing" of the transition state, the computed rate constant is an upper limit to the true rate constant, and the difference due to recrossing may well be the ultimate limit on achievable accuracy. The performance of VPT2 seems to be quite adequate for this reaction, but it is not known how well it will perform in general. For extremely nonquadratic barriers and for very strong multidimensional curvature along the reaction path, higher-order VPT may be needed. In fact, perturbation theory may converge only locally.

In the computational implementation of SCTST distributed as part of the MultiWell Program Suite,[47,48] provision is provided for choosing to treat some internal degrees of freedom as separable. These include free and hindered internal rotations, as well as separable anharmonic vibrations. This pragmatic approach is not well-founded in theory but seems to constitute a reasonable approximation. The current implementation of VPT2 in the CFOUR computer code is based on Cartesian coordinates, but curvilinear coordinates would provide better separability for large-amplitude motions and would provide a better theoretical foundation for treating some modes as separable. However, it is unclear how one would formulate SCTST in such a coordinate system; it would be, at least, a very challenging task.

Much remains to be learned about the optimal way to carry out SCTST calculations. For example, unpublished calculations carried in the course of this work suggest that the accuracy of SCTST is particularly sensitive to the accuracy of the computed imaginary frequency. Thus, it may be necessary to use a high level of theory and extrapolate to the complete basis set limit. Another limitation is that HEAT may not always perform this well, in general, and is not feasible for large systems.[38−40] Nonetheless, judicious adjustment of the energy barrier promises a means for achieving very good fits to experimental data when the ab initio energies are not sufficient.

In summary, SCTST as developed by Miller and co-workers[4−7] is a powerful version of transition-state theory. It includes ZPE and quantum tunneling along the multidimensional reaction path. It allows for complete nonseparability of all internal coordinates, including the reaction coordinate. It can be used to compute both canonical (thermal) and microcanonical (energy-dependent) rate constants, such as those needed for master equation calculations. In the present work, SCTST has been combined with the HEAT theory[38−40] for obtaining highly accurate energies. The fully ab initio theoretical thermal rate constants obtained in this work are in excellent agreement with the extensive experimental rate data for this highly nonclassical reaction. Thus, this work provides strong evidence that TST is valid when recrossing can be neglected. Further work is needed to define the limitations of the theory and to identify the optimal choices for carrying out the calculations, but in our opinion, it is a very promising method.

■ ASSOCIATED CONTENT

Supporting Information. Calculated energies, harmonic and anharmonic zero-point energies, spectroscopic parameters, and anharmonic constants. This material is available free of charge via the Internet at http://pubs.acs.org.

■ AUTHOR INFORMATION

Corresponding Author

*E-mail: jrbarker@umich.edu.

Notes

§E-mail: nguyenlt@umich.edu (T.L.N.); jfstanton@mail.utexas.edu (J.F.S.).

■ ACKNOWLEDGMENT

T.L.N. and J.R.B. thank NSF (Atmospheric and Geospace Sciences) and NASA (Upper Atmosphere Research Program), and J.F.S. thanks the Robert A. Welch Foundation (Grant F-1283) and NSF for support of this research.

■ REFERENCES

(1) Smith, I. W. M.; Crim, F. F. *Phys. Chem. Chem. Phys.* **2002**, *4*, 3543–3551.
(2) Castillo, J. F. *ChemPhysChem* **2002**, *3*, 320–332.
(3) Nguyen, T. L.; Stanton, J. F.; Barker, J. R. *Chem. Phys. Lett.* **2010**, *499*, 9–15.
(4) Miller, W. H. *J. Chem. Phys.* **1975**, *62*, 1899–1906.

(5) Miller, W. H. *Faraday Discuss. Chem. Soc.* **1977**, *62*, 40–46.
(6) Miller, W. H.; Hernandez, R.; Handy, N. C.; Jayatilaka, D.; Willets, A. *Chem. Phys. Lett.* **1990**, *172*, 62–68.
(7) Hernandez, R.; Miller, W. H. *Chem. Phys. Lett.* **1993**, *214*, 129–136.
(8) Mills, I. M. Vibration−Rotation Structure in Asymmetric- and Symmetric-Top Molecules. In *Molecular Spectroscopy: Modern Research*; Rao, K. N., Mathews, C. W., Eds.; Academic Press: New York, 1972; Vol. 1, pp 115−140.
(9) Fernandez-Ramos, A.; Ellingson, B. A.; Garrett, B. C.; Truhlar, D. G. *Rev. Comput. Chem.* **2007**, *23*, 125–232.
(10) Zheng, J.; Zhang, S.; Lynch, B. J.; Corchado, J. C.; Chuang, Y. Y.; Fast, P. L.; Hu, W. P.; Liu, Y. P.; Lynch, G. C.; Nguyen, K. A.; Jackels, C. F.; Ramos, A. F.; Ellingson, B. A.; Melissas, V. S.; Villa, J.; Rossi, I.; Coition, E. L.; Pu, J.; Albu, T. V.; Steckler, R.; Garrett, B. C.; Isaacson, A. D.; Truhlar, D. G. *POLYRATE-v2008* version 2008 ed.; University of Minnesota: Minneapolis, MN, 2008.
(11) Pieterse, G.; Krol, M. C.; Röckmann, T. *Atmos. Chem. Phys.* **2009**, *9*, 8503–8529.
(12) Miller, J. A.; Pilling, M. J.; Troe, E. *Proc. Combust. Inst.* **2005**, *30*, 43–88.
(13) Balat, M. *Energy Sources* **2009**, *31*, 39–50.
(14) Rahn, T.; Eller, J. M.; Boering, K. A.; Wennberg, P. O.; McCarthy, M. C.; Tyler, S.; Schauffer, S.; Donnelly, S.; Atlas, E. *Nature* **2003**, *424*, 918–921.
(15) Strazisar, B. R.; Lin, C.; Davis, H. F. *Science* **2000**, *290*, 958–961.
(16) Smith, I. W. M.; Zellner, R. *J. Chem. Soc., Faraday Trans. 2* **1973**, *69*, 1617.
(17) Ravishankara, R.; Nicovich, J. M.; Thompson, R. L.; Tully, F. P. *J. Phys. Chem.* **1981**, *85*, 2498.
(18) Talukdar, R. K.; Gierczak, T.; Goldfarb, L.; Rudich, Y.; Rao, B. S. M.; Ravishankara, R. *J. Phys. Chem.* **1996**, *100*, 3037.
(19) Krasnoperov, L. N.; Michael, J. V. *J. Phys. Chem. A* **2004**, *108*, 5643–5648.
(20) Orkin, V. L.; Kozlov, S. N.; Poskrebyshev, G. A.; Kurylo, M. J. *J. Phys. Chem. A* **2006**, *110*, 6978–6985.
(21) Truong, T. N.; Evans, T. J. *J. Phys. Chem.* **1994**, *98*, 9558–9564.
(22) Truong, T. N. *J. Chem. Phys.* **1995**, *102*, 5335–5341.
(23) Matzkies, F.; Manthe, U. *J. Chem. Phys.* **1998**, *108*, 4828–4836.
(24) Garcia, E.; Saracibar, A.; Rodriquez, A.; Lagara, A.; Lendvay, G. *Mol. Phys.* **2006**, *104*, 839–846.
(25) Tian, X.; Gao, T.; He, N.; Zhang, Z. *Chem. Phys.* **2008**, *354*, 142–147.
(26) Sierra, J. D.; Martinez, R.; Hernando, J.; Gonzalez, M. *Phys. Chem. Chem. Phys.* **2009**, *11*, 11520–11527.
(27) Espinosa-Garcia, J.; Bonnet, L.; Corchado, J. C. *Phys. Chem. Chem. Phys.* **2010**, *12*, 3873–3877.
(28) Wu, G. S.; Schatz, G. C.; Lendway, G.; Fang, D. C.; Harding, L. B. *J. Chem. Phys.* **2000**, *113*, 3150–3161.
(29) Yang, M.; Zhang, D. H.; Collins, M. A.; Lee, S. Y. *J. Chem. Phys.* **2001**, *114*, 4759–4762.
(30) Zhang, D. H.; Yang, M.; Lee, S.-Y. *J. Chem. Phys.* **2001**, *114*, 8733–8736.
(31) Zhang, D. H.; Yang, M.; Lee, S.-Y. *J. Chem. Phys.* **2002**, *116*, 2388–2394.
(32) Garcia, E.; Saracibar, A.; Sanchez, C.; Lagana, A. *Chem. Phys.* **2005**, *308*, 201–210.
(33) Troya, D.; Lakin, M. J.; Schatz, G. C.; Gonzalez, M. *J. Chem. Phys.* **2001**, *115*, 1828–1842.
(34) Defazio, P.; Gray, S. K. *J. Phys. Chem. A* **2003**, *107*, 7132–7137.
(35) Chakraborty, A.; Truhlar, D. G. *Proc. Natl. Acad. Sci. U.S.A.* **2005**, *102*, 6744–6749.
(36) Raghavachari, K.; Trucks, G. W.; Pople, J. A.; Head-Gordon, M. *Chem. Phys. Lett.* **1989**, *157*, 479.
(37) Almlof, J.; Taylor, P. R. *J. Chem. Phys.* **1987**, *86*, 4070–4077.
(38) Tajti, A.; Szalay, P. G.; Csaszar, A. G.; Kallay, M.; Gauss, J.; Valeev, E. F.; Flowers, B. A.; Vazquez, J.; Stanton, J. F. *J. Chem. Phys.* **2004**, *121*, 11599–11613.
(39) Bomble, Y. J.; Vazquez, J.; Kallay, M.; Michauk, C.; Szalay, P. G.; Csaszar, A. G.; Gauss, J.; Stanton, J. F. *J. Chem. Phys.* **2006**, *125*, 064108.
(40) Harding, M. E.; Vazquez, J.; Ruscic, B.; Wilson, A. K.; Gauss, J.; Stanton, J. F. *J. Chem. Phys.* **2008**, *128*, 114111.
(41) Frisch, M. J.; Trucks, G. W.; Schlegel, H. B.; Scuseria, G. E.; Robb, M. A.; Cheeseman, J. R.; Scalmani, G.; Barone, V.; Mennucci, B.; Petersson, G. A.; Nakatsuji, H.; Caricato, M.; Li, X.; Hratchian, H. P.; Izmaylov, A. F.; Bloino, J.; Zheng, G.; Sonnenberg, J. L.; Hada, M.; Ehara, M.; Toyota, K.; Fukuda, R.; Hasegawa, J.; Ishida, M.; Nakajima, T.; Honda, Y.; Kitao, O.; Nakai, H.; Vreven, T.; J. A. Montgomery, J.; Peralta, J. E.; Ogliaro, F.; Bearpark, M.; Heyd, J. J.; Brothers, E.; Kudin, K. N.; Staroverov, V. N.; Kobayashi, R.; Normand, J.; Raghavachari, K.; Rendell, A.; Burant, J. C.; Iyengar, S. S.; Tomasi, J.; Cossi, M.; Rega, N.; Millam, J. M.; Klene, M.; Knox, J. E.; Cross, J. B.; Bakken, V.; Adamo, C.; Jaramillo, J.; Gomperts, R.; Stratmann, R. E.; Yazyev, O.; Austin, A. J.; Cammi, R.; Pomelli, C.; Ochterski, J. W.; Martin, R. L.; Morokuma, K.; Zakrzewski, V. G.; Voth, G. A.; Salvador, P.; Dannenberg, J. J.; Dapprich, S.; Daniels, A. D.; Farkas, O.; Foresman, J. B.; Ortiz, J. V.; Cioslowski, J.; Fox, D. J. *Gaussian 09*, revision A.1; Gaussian, Inc.: Wallingford, CT, 2009.
(42) Stanton, J. F.; Gauss, J.; Harding, M. E.; Szalay, P. G. with contributions from Auer, A. A.; Bartlett, R. J.; Benedikt, U.; Berger, C.; Bernholdt, D. E.; Bomble, Y. J.; Christiansen, O.; Heckert, M.; Heun, O.; Huber, C.; Jagan, T.-C.; Jonsson, D.; Jusélius, J.; Klein, K.; Lauderdale, W. J.; Matthews, D. A.; Metzroth, T.; O'Neill, D. P.; Price, D. R.; Prochnow, E.; Ruud, K.; Schiffmann, F.; Stopkowicz, S.; Vázquez, J.; Wang, F.; Watts, J. D. and the integral packages MOLECULE (Almlöf, J.; Taylor, P. R.), PROPS (Taylor, P. R.), and ABACUS (Helgaker, T.; Jensen, H. J. Aa.; Jørgensen, P.; Olsen, J.), and ECP routines by Mitin, A. V.; van Wüllen, C. *CFOUR*, a quantum chemical program package; 2009; see http://www.cfour.de/.
(43) Truhlar, D. G.; Isaacson, A. D. *J. Chem. Phys.* **1990**, *94*, 357–359.
(44) Wang, F.; Landau, D. P. *Phys. Rev. Lett.* **2001**, *86*, 2050–2053.
(45) Basire, M.; Parneix, P.; Calvo, F. *J. Chem. Phys.* **2008**, *129*, 081101.
(46) Nguyen, T. L.; Barker, J. R. *J. Phys. Chem. A* **2010**, *114*, 3718–3730.
(47) Barker, J. R. *Int. J. Chem. Kinet.* **2001**, *33*, 232–245.
(48) Barker, J. R.; Ortiz, N. F.; Preses, J. M.; Lohr, L. L.; Maranzana, A.; Stimac, P. J.; Nguyen, T. L.; Kumar, T. J. D. *MultiWell-2010.2 Software*; University of Michigan: Ann Arbor, Michigan, 2010; (http://aoss.engin.umich.edu/multiwell/).
(49) Wigner, E. *Z. Physik. Chem.* **1932**, *B19*, 203–216.
(50) Eckart, C. *Phys. Rev.* **1930**, *35*, 1303–1309.
(51) Johnston, H. S.; Heicklen, J. *J. Phys. Chem.* **1962**, *99*, 532–533.
(52) Johnston, H. S. *Gas Phase Reaction Rate Theory*; Ronald Press Co.: New York, 1966.
(53) Marcus, R. A. *J. Chem. Phys.* **1966**, *45*, 4493–4499.
(54) Truhlar, D. G.; Kuppermann, A. *J. Chem. Phys.* **1972**, *56*, 2232–2252.
(55) George, T. F.; Miller, W. H. *J. Chem. Phys.* **1972**, *57*, 2458–2457.
(56) Marcus, R. A. *J. Chem. Phys.* **1966**, *45*, 2138.
(57) Miller, W. H. *Acc. Chem. Res.* **1976**, *9*, 306–312.
(58) Smith, I. W. M.; Zellner, R. *J. Chem. Soc., Faraday Trans. 2* **1974**, *8*, 1045.
(59) Paraskevopoulos, G.; Nip, W. S. *Can. J. Chem.* **1980**, *58*, 2146.
(60) Vaghjiani, G. L.; Ravishankara, A. R.; Cohen, N. *J. Phys. Chem.* **1989**, *93*, 7833.